

Reparameterization Proximal Policy Optimization

Hai Zhong, Xun Wang, Zhuoran Li, and Longbo Huang *

Institute for Interdisciplinary Information Sciences (IIIS), Tsinghua University
{zhongh22,wang-x24,lizr20}@mails.tsinghua.edu.cn, longbohuang@tsinghua.edu.cn

Abstract

By leveraging differentiable dynamics, Reparameterization Policy Gradient (RPG) achieves high sample efficiency. However, current approaches are hindered by two critical limitations: the under-utilization of computationally expensive dynamics Jacobians and inherent training instability. While sample reuse offers a remedy for under-utilization, no prior principled framework exists, and naive attempts risk exacerbating instability. To address these challenges, we propose Reparameterization Proximal Policy Optimization (RPO). We first establish that under sample reuse, RPG naturally optimizes a PPO-style surrogate objective via Backpropagation Through Time, providing a unified framework for both on- and off-policy updates. To further ensure stability, RPO integrates a clipped policy gradient mechanism tailored for RPG and employs explicit Kullback-Leibler divergence regularization. Experimental results demonstrate that RPO maintains superior sample efficiency and consistently outperforms or achieves state-of-the-art performance across diverse tasks.

1 Introduction

Reparameterization Policy Gradient (RPG) [16, 1] is a policy gradient method that computes the policy gradient using the reparameterization trick [11, 24]. Unlike REINFORCE [32, 31], RPG directly backpropagates through the trajectory to obtain a policy gradient estimate. This approach has become increasingly attractive with the recent rise of differentiable simulators [8, 34, 33, 35]. The applicability of RPG methods extends across a broad spectrum of robotic domains, including autonomous driving, quadrupedal locomotion, and agile flight [28, 18, 39]. Notably, the exceptional sample efficiency of RPG has driven breakthroughs in training policies directly in physical environments, as exemplified by recent achievements in real-world quadrotor flight [19].

However, existing RPG-based approaches face two primary challenges. First, backpropagating through system dynamics is computationally expensive due to the calculation of dynamics Jacobians. Yet, prior on-policy methods lack a sample reuse mechanism (more specifically, reusing dynamics Jacobians): they dis-

* Corresponding Author

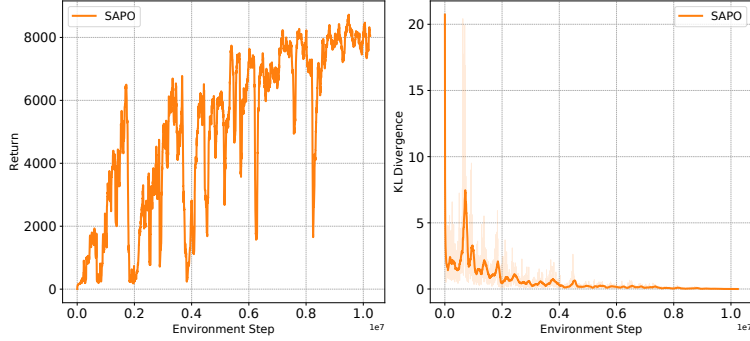


Figure 1: An example of SAPO’s training instability in the Humanoid task. Large KL divergence (both smoothed and raw curves shown on the right) spikes correspond to sudden performance drops. Additional examples of training instability for both SAPO and SHAC are provided in Appendix K.

card costly dynamics Jacobians after a single policy update. Reusing these computationally expensive dynamics Jacobians could further boost RPG’s sample efficiency and shorten the wall-clock training time of RPG-based approaches. Sample reuse is particularly desirable for learning RL policies in the real world with RPG, where data collection is time-consuming and fully utilizing each sample is paramount.

Second, RPG is notoriously prone to optimization instability, often suffering from exploding or vanishing gradients in environments with non-smooth dynamics or long horizons [15, 29]. Even with state-of-the-art (SOTA) variance reduction techniques, such as short-horizon rollouts in SHAC [34] and entropy regularization in SAPO [33], we empirically observe that RPG suffers from training instability, as shown in Figure 1. This creates a dilemma: while sample reuse is desirable for efficiency, it inherently exacerbates optimization instability since it increases the update-to-data ratio, necessitating an explicit mechanism to constrain policy updates.

In this work, we propose **Reparameterization Proximal Policy Optimization (RPO)** to address these limitations. First, we establish a principled sample reuse mechanism for RPG. This is achieved by demonstrating that, under sample reuse, RPG naturally aligns with a PPO-like surrogate objective via backpropagation through time (BPTT) [17], providing a unified framework for both on- and off-policy updates. This formulation enables RPO to achieve high sample efficiency. Second, to maintain stability even with sample reuse, RPO incorporates a clipped policy gradient mechanism tailored to the specific characteristics of RPG, which constrains updates driven by large importance weights. Furthermore, we enhance stability via an explicit KL divergence regularization term, as we empirically observe that clipping alone is insufficient. Finally, RPO remains fully compatible with and benefits from existing variance reduction methods for RPG.

We conduct experiments on a suite of locomotion and manipulation tasks using two differentiable simulators, DFlex [34, 3] and Rewarped [33]. Experimental results show that RPO achieves superior sample efficiency and consistently achieves state-of-the-art performances across all tasks. We believe RPO’s sample reuse mechanism holds great promise for future RPG-based applications in learning real-world RL policies, as utilizing each rollout trajectory to its full potential is clearly critical.

To summarize, our main contributions are: **(i)** We show that with the sample reuse mechanism, RPG is nat-

usually linked to a PPO-like surrogate objective, providing a unified framework for both on- and off-policy updates. **(ii)** We propose **Reparameterization Proximal Policy Optimization**, which achieves stable and sample-efficient learning by synergizing sample reuse with a tailored importance weight clipping mechanism and explicit KL regularization. **(iii)** We conduct extensive experiments on a suite of locomotion and manipulation tasks using the differentiable simulators DFlex and Rewarped, demonstrating RPO’s high sample efficiency and strong performance.

2 Related Work

Policy Gradient Estimators. One classical class of policy gradient estimators is based on the score function, such as the REINFORCE gradient estimator [32, 31]. Many policy gradient methods, such as PPO and TRPO [26, 25], rely on variants of the REINFORCE gradient estimator. One limitation of the REINFORCE gradient is its high variance, which results in low sample efficiency. On the other hand, if one has access to the underlying dynamic model, either through differentiable simulators [34, 8, 33] or learned world models [6, 1], another type of policy gradient named Reparameterization Policy Gradient, which is based on the reparameterization trick [11, 24], can be obtained. Using the reparameterization trick [11, 24], RPG directly backpropagates through the trajectory and obtains an unbiased estimate of the policy gradient. By contrast, the REINFORCE gradient estimator does not need to backpropagate through the entire computational graph and only relies on local computation [21]. Since RPG utilizes the gradients of the dynamics model, RPG typically enjoys less variance than the REINFORCE gradient estimator [16].

RPG-based Reinforcement Learning Algorithms. It is well known that RPG obtained by vanilla backpropagation through time over a long time horizon suffers from the vanishing/exploding gradient problem [29, 15, 37, 13]. This phenomenon is amplified when dealing with stiff dynamics, such as contact [36, 29, 40, 20]. RPG can exhibit a large variance when the gradient magnitude is large, which renders the underlying reinforcement learning algorithm unstable, struggling with non-convex loss landscapes.

Several works [22, 23, 29] weight and combine RPG and REINFORCE according to their variance, while AGPO [2] further combines RPG with gradients of Q-functions. SHAC and AHAC [34, 3] reduce the variance of RPG by only backpropagating through a truncated length of the trajectory, aided by a value function to estimate future returns. MB-MIX [38] backpropagates a mixture of trajectories with different lengths to better balance the bias-variance trade-off. GI-PPO [27] first optimizes the policy using RPG, then uses the REINFORCE gradient to perform further off-policy updates in the PPO style. However, the gradients computed by REINFORCE are not only of lower quality than those from RPG, but can also conflict with each other, thereby degrading sample efficiency and performance. Entropy is also introduced to regularize RPG-based policy updates and promote exploration [33, 1].

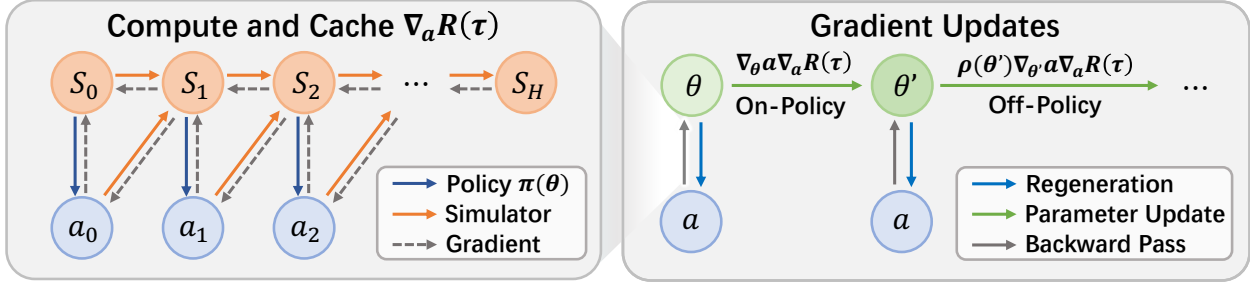


Figure 2: Computing the reparameterization policy gradient of the surrogate objective involves three steps: **(a)** Action-gradients are computed from rollouts via a single backward pass and cached. **(b)** These gradients are used directly for the initial, on-policy update. **(c)** For subsequent off-policy updates, the cached action-gradients are importance-weighted by $\rho(\theta')$ and reused, enabling stable sample reuse. Note that we only plot the trajectory for H steps for illustration purposes.

3 Preliminaries

3.1 Reinforcement Learning Formulation

In this work, we consider problems formulated as a Markov Decision Process (MDP) [30]. An MDP is formally defined by a tuple $(\mathcal{S}, \mathcal{A}, p, r, p_0, \gamma)$, where \mathcal{S} is the set of states, \mathcal{A} is the set of actions, $p : \mathcal{S} \times \mathcal{A} \times \mathcal{S} \rightarrow [0, 1]$ is the state transition probability function, $r : \mathcal{S} \times \mathcal{A} \rightarrow \mathbb{R}$ is the reward function, s_0 is the initial state, $p_0(s_0)$ is the initial state distribution, and $\gamma \in [0, 1)$ is the discount factor.

The goal of reinforcement learning (RL) is to find the optimal parameter θ^* for a parameterized stochastic policy π_θ . A parameterized stochastic policy $\pi_\theta(a|s)$ specifies the probability distribution over actions $a \in \mathcal{A}$ given a state $s \in \mathcal{S}$. The optimal parameter θ^* maximizes the expected discounted cumulative reward:

$$\theta^* = \arg \max_{\theta} J(\theta) = \arg \max_{\theta} \mathbb{E}_{\tau \sim \pi_\theta} [R(\tau)] \quad (1)$$

where $\tau = (s_0, a_0, s_1, a_1, \dots)$ is the trajectory generated by following the policy π_θ . Here, $r(s_t, a_t)$ denotes the reward received at time step t , and $R(\tau) = \sum_{t=0}^{\infty} \gamma^t r(s_t, a_t)$ is the discounted cumulative reward for the trajectory τ .

3.2 Reparameterization Policy Gradient

RPG uses the reparameterization trick [11, 24, 5] to sample an action a_t from a Gaussian policy $\pi_\theta(a_t|s_t)$. Specifically, the policy network first predicts the mean $\mu_\theta(s_t)$ and standard deviation $\sigma_\theta(s_t)$, and then combines them with a reparameterization noise ϵ_t at time step t :

$$a_t = \mu_\theta(s_t) + \sigma_\theta(s_t) \cdot \epsilon_t, \quad \text{where } \epsilon_t \sim \mathcal{N}(0, \mathcal{I}). \quad (2)$$

We denote this transformation as $a_t = f_\theta(\epsilon_t; s_t)$.

We focus on deterministic system dynamics $s_{t+1} = g(s_t, a_t)$. Consistent with prior works [34, 3, 33], we

adopt the following assumption regarding the dynamics and rewards to guarantee well-defined reparameterization policy gradients.

Assumption 1. The system dynamics $g(s, a)$ and the reward function $r(s, a)$ are differentiable w.r.t. state s and action a .

With the reparameterization trick, RPG can backpropagate through dynamics by computing Jacobians, $\frac{\partial s_{t+1}}{\partial a_t}$ and $\frac{\partial s_{t+1}}{\partial s_t}$, to obtain a policy gradient estimate:

$$\nabla_{\theta} J(\theta) = \mathbb{E}_{s_0, \epsilon_0, \epsilon_1, \dots} [\nabla_{\theta} R(\tau)]. \quad (3)$$

Note that the expectation is taken with respect to the initial state distribution and sampled noise at different time steps.

However, full backpropagation through long trajectories could lead to high gradient variance and unstable training. Short-Horizon Actor-Critic (SHAC) [34], addresses this by backpropagating through only a short horizon of the trajectory, using a value function to capture the long-term return. SHAC’s variant of RPG is as follows:

$$\mathbb{E}_{s_0, \epsilon_0, \epsilon_1, \dots} [\nabla_{\theta} [R(\tau_{t_0:t_0+h-1}) + \gamma^h V(s_{t_0+h})]], \quad (4)$$

where t_0 is the starting time step for the trajectory, h is the short horizon, $R(\tau_{t_0:t_0+h-1})$ is the cumulative reward of the trajectory within the short horizon, and $V(s_{t_0+h})$ is the value function’s estimate of the future return.

3.3 Surrogate Objective

PPO [26] and TRPO [25] optimize variants of the following surrogate objective function [10]:

$$\begin{aligned} L_{\pi_{\theta_{\text{old}}}}(\theta) &= \int_s \sum_{t=0}^{\infty} \gamma^t p(s_t = s | \pi_{\theta_{\text{old}}}) \int_a A^{\pi_{\theta_{\text{old}}}}(s, a) \pi_{\theta}(a | s) da ds \end{aligned} \quad (5)$$

where $\pi_{\theta_{\text{old}}}$ is the behavior policy used to collect samples; $\sum_{t=0}^{\infty} \gamma^t p(s_t = s | \pi_{\theta_{\text{old}}})$ is the unnormalized state probability density induced by $\pi_{\theta_{\text{old}}}$; and $A^{\pi_{\theta_{\text{old}}}}(s, a)$ is the advantage function corresponding to $\pi_{\theta_{\text{old}}}$. This objective measures the performance of the new policy π_{θ} , using the state distribution and advantages for the behavior policy $\pi_{\theta_{\text{old}}}$. PPO optimizes a clipped variant of this objective, while TRPO optimizes an explicit KL-constrained variant [26, 25].

By the law of the unconscious statistician [4], we can rewrite the surrogate objective in the reparameterization form:

$$\begin{aligned} L_{\pi_{\theta_{\text{old}}}}(\theta) &= \int_s d^{\pi_{\theta_{\text{old}}}}(s) \int_{\epsilon} A^{\pi_{\theta_{\text{old}}}}(s, a)|_{a=f_{\theta}(\epsilon; s)} p_{\text{std}}(\epsilon) d\epsilon ds \end{aligned} \quad (6)$$

where $d^{\pi_{\theta_{\text{old}}}}(s)$ denotes the unnormalized state density induced by $\pi_{\theta_{\text{old}}}$ and $p_{\text{std}}(\epsilon)$ is the probability den-

sity function for standard Gaussian distribution. This surrogate objective differs fundamentally from the objective of the stochastic value gradient (SVG) [7, 1], as equation 6 measures performance using the value function of the behavior policy, while SVG uses that of the current policy.

4 Reparameterization Proximal Policy Optimization

In this section, we introduce our proposed method: Reparameterization Proximal Policy Optimization. First, we show that with sample reuse (i.e., reusing computed action-gradients obtained via backpropagation through dynamics), RPG is indeed calculating the reparameterization policy gradient for the surrogate objective (equation equation 6). This provides a unified framework for both on- and off-policy updates for RPG. Based on this insight, we propose RPO to achieve stable sample reuse. RPO incorporates three key mechanisms: (i) optimizing the PPO-like surrogate objective via RPG, (ii) a policy gradient clipping mechanism designed for RPG, and (iii) an explicit KL regularization term. The overall algorithm is summarized in Algorithm 1.

4.1 Surrogate Objective for Policy Improvement

State-of-the-art RPG methods, e.g., [34, 33], are limited to a single policy update per batch, underutilizing expensive BPTT gradients. While GI-PPO [27] attempts sample reuse, it relies on REINFORCE gradients for off-policy updates, failing to utilize dynamics Jacobians. Its hybrid REINFORCE approach could introduce update conflicts and underutilize the low-variance RPG gradients.

We establish a novel connection showing that sample reuse in RPG (i.e., reusing action-gradients computed via BPTT) is equivalent to calculating the reparameterization policy gradient for the surrogate objective, thereby providing a unified framework for both on- and off-policy updates.

Therefore, we introduce the first key component of RPO, the surrogate objective for policy improvement:

$$L_{\pi_{\theta_{\text{old}}}}(\theta) = \mathbb{E}_{s \sim d^{\pi_{\theta_{\text{old}}}}, \epsilon \sim p_{\text{std}}} [A^{\pi_{\theta_{\text{old}}}}(s, f_{\theta}(\epsilon; s))] \quad (7)$$

where $\pi_{\theta_{\text{old}}}$ is the policy before the update, $d^{\pi_{\theta_{\text{old}}}}(s)$ denotes the unnormalized state density induced by $\pi_{\theta_{\text{old}}}$, and ϵ is sampled from the standard Gaussian distribution. We show that computing the reparameterization policy gradient for the surrogate objective is equivalent to reusing the action-gradient computed via BPTT, enabling sample reuse.

The reparameterization policy gradient of the surrogate objective with respect to policy parameter θ is as

follows:

$$\nabla_{\theta} L_{\pi_{\theta_{\text{old}}}}(\theta) \tag{8}$$

$$\begin{aligned} &= \int_s d^{\pi_{\theta_{\text{old}}}}(s) \int_{\epsilon} [\nabla_{\theta} a \nabla_a A^{\pi_{\theta_{\text{old}}}}(s, a)|_{a=f_{\theta}(\epsilon; s)} p_{\text{std}}(\epsilon)] d\epsilon ds \\ &= \int_s d^{\pi_{\theta_{\text{old}}}}(s) \int_{\epsilon} [\nabla_{\theta} a \nabla_a Q^{\pi_{\theta_{\text{old}}}}(s, a)|_{a=f_{\theta}(\epsilon; s)} p_{\text{std}}(\epsilon)] d\epsilon ds. \end{aligned} \tag{9}$$

Here $A^{\pi_{\theta_{\text{old}}}}(s, a) = Q^{\pi_{\theta_{\text{old}}}}(s, a) - V^{\pi_{\theta_{\text{old}}}}(s)$ and $V^{\pi_{\theta_{\text{old}}}}(s)$ is constant with respect to the parameter θ being optimized. Note that $\nabla_a A^{\pi_{\theta_{\text{old}}}}(s, a) = \nabla_a Q^{\pi_{\theta_{\text{old}}}}(s, a)$, since the value function $V^{\pi_{\theta_{\text{old}}}}(s)$ does not depend on actions. Also, equation (8) is rewritten for taking expectation over the whole trajectory as equation (16) in Appendix D.

4.1.1 Deriving the Reparameterization Gradient via Action-Gradient Reuse

In this section, we show that computing the RPG for the surrogate objective naturally leads to reusing action-gradients for multiple policy updates (more details for this derivation are given in Appendix D).

As the first step, we collect a batch of rollouts with the behavior policy, setting $\pi_{\theta_{\text{old}}} = \pi_{\theta}$. To illustrate the connection, we consider the resulting infinite-horizon computational graph. We consider the gradients of the discounted cumulative return with respect to the action at each time step. From here, we clearly see that the action-gradient for time step k , $\nabla_{a_k} R(\tau) = \gamma^k \nabla_{a_k} \sum_{t=k}^{\infty} \gamma^{(t-k)} r(s_t, a_t)$, is exactly an unbiased Monte Carlo estimate of $\gamma^k \nabla_a Q^{\pi_{\theta_{\text{old}}}}(s_k, a_k)$, where s_k and a_k are sampled according to $p(s_k = s | \pi_{\theta_{\text{old}}})$ and $\pi_{\theta_{\text{old}}}(a_k | s_k)$. This holds because the reparameterization trick allows us to express $\gamma^k \nabla_a Q^{\pi_{\theta_{\text{old}}}}(s_k, a_k)$ as the expected gradient of the returns with respect to a_k across all possible paths sampled via the reparameterization noise (as we assume deterministic dynamics). As shown in Figure 2, we cache these action-gradients for subsequent calculations (note that we only plot the trajectory for H steps for illustration purposes).

On-policy reparameterization policy gradient: In the first update epoch, the behavior policy $\pi_{\theta_{\text{old}}}$ is identical to the current policy π_{θ} . We compute the on-policy gradient by backpropagating the cached action-gradients through the policy network θ , as depicted in Figure 2. Summing over different time steps and taking the average over the batch of trajectories, gives an unbiased Monte Carlo estimate of the surrogate objective’s on-policy gradient: $\int_s d^{\pi_{\theta_{\text{old}}}}(s) \int_{\epsilon} [\nabla_{\theta} a \nabla_a Q^{\pi_{\theta_{\text{old}}}}(s, a)|_{a=f_{\theta}(\epsilon; s)} p_{\text{std}}(\epsilon)] d\epsilon ds$. This holds since: (i) s_k is sampled from $p(s_k = s | \pi_{\theta_{\text{old}}})$, (ii) a_k is generated via $a_k = f_{\theta_{\text{old}}}(\epsilon; s_k)$ with $\epsilon \sim p_{\text{std}}(\epsilon)$, and (iii) $\pi_{\theta_{\text{old}}}$ coincides with π_{θ} for this first epoch.

Off-policy reparameterization policy gradient: The on-policy gradient estimate can be used to update the policy parameters from θ to θ' . After this update, the behavior policy $\pi_{\theta_{\text{old}}}$ (which generated the data) is now different from the current policy $\pi_{\theta'}$. Now we must compute the off-policy RPG gradient. As we would show, this naturally leads to reusing the action-gradients computed via BPTT.

We can reuse the exact same cached action-gradients $\nabla_{a_k} R(\tau)$, but we must re-establish a computational path from the new policy parameters θ' to the action a_k to compute $\nabla_{\theta'} a_k$. We achieve this by regenerating

the noise ϵ_{reg} that is required for the current policy to produce a_k . This allows us to express the action as $a_k = f_{\theta'}(\epsilon_{\text{reg}}; s_k)$, creating a new differentiable path.

As shown in Figure 2, the cached action-gradients are then backpropagated through this new path, yielding an estimate of $\gamma^k \nabla_{\theta'} a_k \nabla_{a_k} Q^{\pi_{\theta_{\text{old}}}}(s_k, a_k)|_{a_k=f_{\theta'}(\epsilon_{\text{reg}}; s_k)}$ for each time step. We further weight each time step’s gradient by the importance sampling ratio $\rho(\theta') = \frac{\pi_{\theta'}(a|s)}{\pi_{\theta_{\text{old}}}(a|s)}$, to obtain an unbiased off-policy reparameterization policy gradient estimate for the surrogate objective. A proof for the unbiasedness is given in Proposition 1 in Appendix D.

4.1.2 Practical implementation for policy improvement

In this section, we provide the algorithmic details of the sample reuse mechanism for policy updates, building upon the previous derivations.

Collecting rollouts and computing action-gradients. Following SHAC [34], we collect a batch of N short-horizon trajectories using the current policy π_{θ} and bootstrap future returns via the value estimate of the terminal state. We then employ BPTT to compute and cache the corresponding action gradients for each time step, denoted as $\nabla_a R(\tau)$, where $R(\tau)$ incorporates the terminal value estimate. Note that each trajectory in the batch is only backpropagated through once. As we previously discussed, the action-gradient for a specific time step $\nabla_{a_k} R(\tau)$ is an unbiased estimate of $\gamma^k \nabla_a Q^{\pi_{\theta_{\text{old}}}}(s_k, a_k)$. Since $A^{\pi_{\theta_{\text{old}}}}(s_k, a_k) = Q^{\pi_{\theta_{\text{old}}}}(s_k, a_k) - V^{\pi_{\theta_{\text{old}}}}(s_k)$ and $V^{\pi_{\theta_{\text{old}}}}(s_k)$ does not depend on the action a_k , $\nabla_{a_k} R(\tau)$ is also an unbiased estimate of $\gamma^k \nabla_a A^{\pi_{\theta_{\text{old}}}}(s_k, a_k)$.

On-policy and Off-policy Updates. We perform M optimization epochs on a batch of cached action-gradients. The first update is on-policy, while all subsequent updates ($1 < m \leq M$) are off-policy. Our method for computing the reparameterization policy gradient of the surrogate objective is unified across both cases. For each update step, we perform the following procedure.

First, to compute the gradient for the current policy π_{θ} using off-policy data, we must re-establish a computational path from policy network parameters θ to the actions. We achieve this by computing the noise ϵ_{reg} that is required for the current policy to regenerate the actions stored in the rollout buffer:

$$\epsilon_{\text{reg}} = f_{\theta}^{-1}(a; s), \tag{10}$$

where $f_{\theta}^{-1}(a; s)$ is the inverse of the reparameterization transform. With this recovered noise, we can express the action under the current policy as $a = f_{\theta}(\epsilon_{\text{reg}}; s)$, which creates a new computational graph connecting the current policy parameters θ to the action stored in the buffer. Note that SVG [7] has the same action regeneration mechanism.

Next, we introduce a novel **policy gradient clipping mechanism**, designed specifically for RPG. The proposed policy gradient clipping mechanism serves as a safeguard against numerical instability by filtering out samples with excessive importance weight ratios, thereby preventing action probabilities from becoming critically low. Examples of possibly excessive large importance weight ratios and more details for this

design can be found in Appendix J.

Unlike PPO’s clipping mechanism, our formulation clips the importance weight ratio asymmetrically and does not depend on the sign of the advantage function. This design is crucial because RPG, unlike REINFORCE, does not explicitly increase or decrease the log-likelihood of a specific action.

Specifically, let the importance weight ratio be $\rho(\theta) = \frac{\pi_\theta(a|s)}{\pi_{\theta_{old}}(a|s)}$. The gradient contribution from this action is non-zero only if $\rho(\theta)$ is within the clipping range, and is weighted by $\rho(\theta)$:

$$\begin{cases} \rho(\theta)\nabla_\theta a \nabla_a R(\tau), & \text{if } 1 - c_{low} \leq \rho(\theta) \leq 1 + c_{high}, \\ 0, & \text{otherwise,} \end{cases} \quad (11)$$

where $\nabla_a R(\tau)$ is the cached action-gradient. By performing this step for all actions in the buffer, we obtain the clipped policy gradient for the surrogate objective.

4.2 Regularization Terms

While our importance ratio-based policy gradient clipping mechanism is designed for RPG (as detailed above), we empirically find that clipping alone is insufficient to fully ensure stability. More details are shown in ablation study and Appendix J. Hence, we incorporate a KL regularization [12] term, which penalizes large deviations from the behavior policy:

$$L_{KL}(\theta) = \mathbb{E} [D_{KL}(\pi_{\theta_{old}}(\cdot|s) || \pi_\theta(\cdot|s))]. \quad (12)$$

Note that this regularization only takes effect with sample reuse, as the KL divergence and its gradient are zero for the first on-policy update.

We also include an entropy bonus to encourage exploration [5, 33]:

$$L_{ent}(\theta) = \mathbb{E} [H(\pi_\theta(\cdot|s))], \quad (13)$$

where $H(\pi_\theta(\cdot|s))$ denotes the entropy of π_θ at a given state.

4.3 Overall Policy Training Objective and Policy Update

The overall policy training objective is to maximize a weighted combination of all three components:

$$L_{policy}(\theta) = \lambda_{surr} L_{\pi_{\theta_{old}}}(\theta) - \lambda_{KL} L_{KL}(\theta) + \lambda_{ent} L_{ent}(\theta), \quad (14)$$

where λ_{surr} , λ_{kl} and λ_{ent} are the coefficients for the three terms. The three gradient components (from the surrogate objective and the two regularization terms) are combined according to their coefficients, and the final resulting gradient is used to update the policy parameters.

Algorithm 1: Reparameterization Proximal Policy Optimization (RPO)

```

1: Initialize policy parameters  $\theta$  and value function parameters  $\phi$ .
2: for iteration  $k = 1, 2, \dots, K$  do
3:   Initialize empty buffer  $\mathcal{B}$ .
4:   Collect a batch of short-horizon trajectories by running policy  $\pi_\theta$  in parallel environments and store them in buffer  $\mathcal{B}$ .
5:   // Compute and cache action-gradients
6:   Compute and cache the gradients of the discounted cumulative reward w.r.t. each action:  $\nabla_a R(\tau)$ .
7:   for policy update epochs  $m = 1, 2, \dots, M$  do
8:     Regenerate the actions stored in  $\mathcal{B}$  (Equation equation 10) with  $\pi_\theta$ .
9:     Backpropagate the clipped cached action-gradients to policy network parameters  $\theta$ , weighted by the importance weight ratios (Equation equation 11).
10:    Compute the gradients of the KL divergence and entropy regularization terms (Equations equation 12, equation 13).
11:    Combine the gradients and update the policy network parameters  $\theta$ .
12:  end for
13:  for value update epochs  $l = 1, 2, \dots, L$  do
14:    Update value function parameters  $\phi$  by minimizing the regression loss (Equation equation 15).
15:  end for
16: end for

```

Table 1: Stochastic Evaluation (i.e. sampling actions from the policy distribution) for the final performance after training. Each evaluation consists of 128 episodes for each seed. Results are reported as mean \pm standard deviation.

	Hand Reorient	Hopper	Ant	Humanoid	Anymal
PPO	36.83 \pm 17.50	3940.60 \pm 129.72	4146.00 \pm 164.14	1665.66 \pm 410.93	8244.86 \pm 680.87
GI-PPO	27.19 \pm 20.58	5512.30 \pm 285.90	7805.47 \pm 1159.23	7507.85 \pm 639.52	12260.45 \pm 3650.35
SHAC	174.63 \pm 57.54	5067.18 \pm 299.37	8206.15 \pm 940.46	7744.44 \pm 858.97	14568.97 \pm 652.72
SAPO	213.44 \pm 33.95	5407.79 \pm 4.28	8718.60 \pm 946.94	8603.09 \pm 402.82	14095.90 \pm 82.02
RPO (ours)	237.55 \pm 25.16	5525.57 \pm 3.47	8891.04 \pm 440.39	8637.78 \pm 422.17	15674.12 \pm 316.26

4.4 Value Function Training

The value function network is trained by minimizing the following regression loss [34]:

$$L_\phi = \mathbb{E} \left[\|V_\phi(s) - \hat{V}(s)\|^2 \right], \tag{15}$$

where $V_\phi(s)$ is the estimate of the value function, and $\hat{V}(s)$ is the value target computed by TD- λ [30]. We follow SAPO [33] using the double-critic network and including the mean of the two value functions for computing the value target.

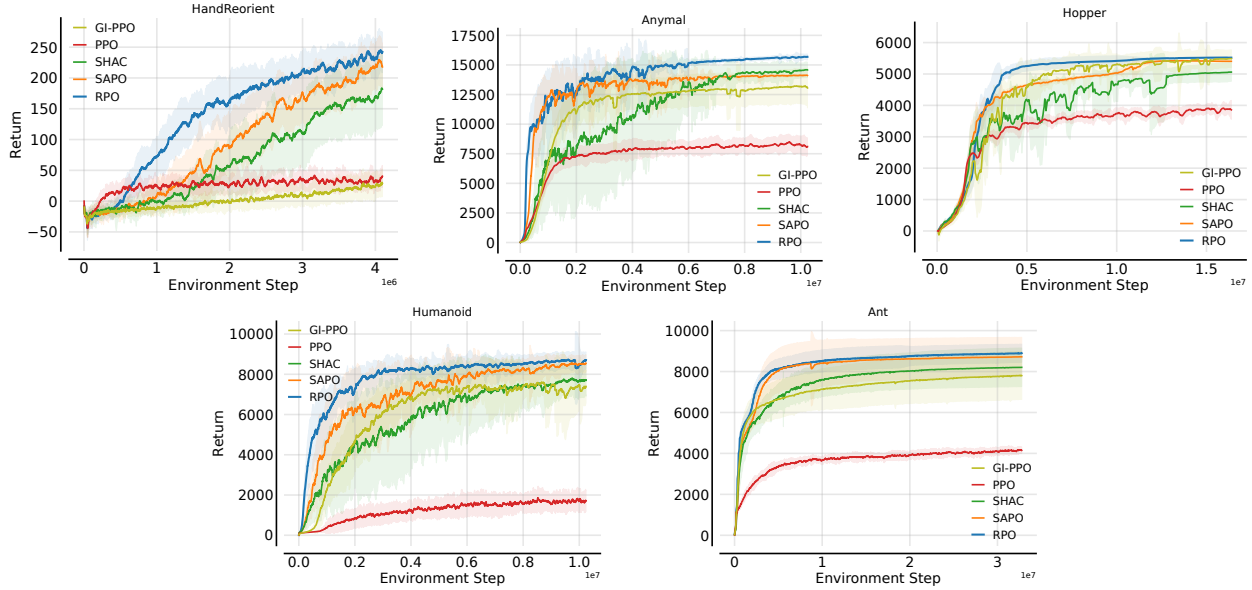


Figure 3: Training performance comparison of RPO, SAPO, SHAC, and PPO. Each plot shows the mean episode return over environment steps, with the shaded region representing the standard deviation. All curves are smoothed with a 100-episode moving average.

5 Experiments

We conduct experiments to answer the following three questions: (i) Does RPO achieve superior sample efficiency compared to previous RPG-based methods? (ii) Does RPO achieve strong performances? (iii) What are the impacts of RPO’s main components on its overall performance?

5.1 Experimental setup

Environments and tasks. We conduct experiments on a suite of five challenging continuous control tasks from two differentiable simulators, DFLex [34, 3] and Rewarped [33]. This suite is composed of four locomotion tasks and one dexterous manipulation task. The four locomotion tasks are from DFLex [3], where

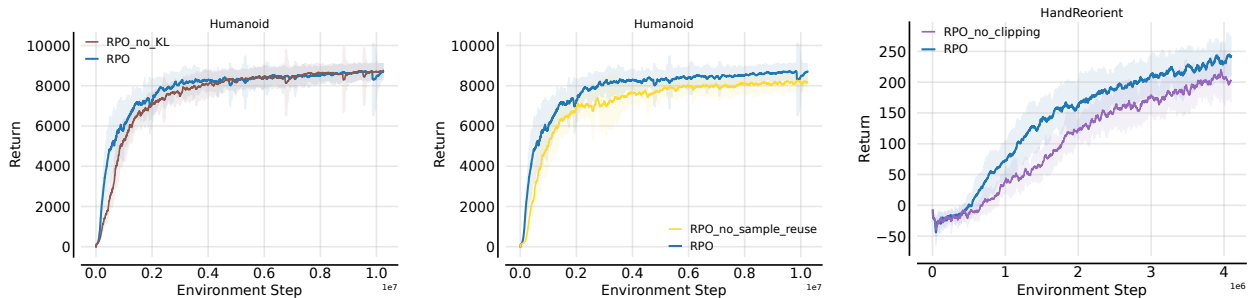


Figure 4: Ablation study of RPO’s components. The plot shows training curves for three variants: RPO without KL regularization, RPO with only one policy update epochs (i.e., no sample reuse), and RPO without the clipping mechanism.

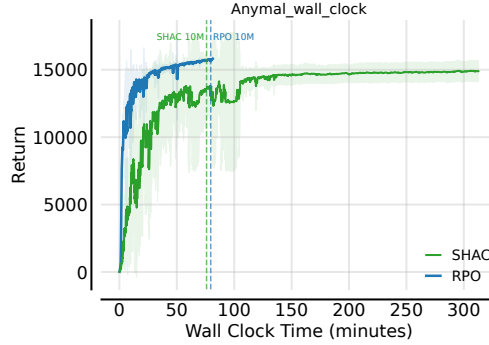


Figure 5: Comparison of wall-clock training time. RPO (10M environment steps) completes training in ~ 81 minutes, compared to ~ 313 minutes for SHAC (40M environment steps). This highlights that the slight computational overhead of sample reuse is far outweighed by the substantial boost in overall training efficiency.

the goal is to maximize the forward velocity: (i) Hopper; (ii) Ant; (iii) Anymal; and (iv) Humanoid. The manipulation task is the Hand Reorient task from Rewarped [33], which involves an Allegro Hand learning to reorient a cube. Further details regarding the environments are provided in Appendix A.

Baselines. We compare the sample efficiency and performance of RPO with SOTA RPG-based and model-free methods: (a) SAPO [33], a SOTA RPG-based method with short-horizon trajectories and entropy regularization; (b) SHAC [34], a variance reduction method for RPG, for which we use the implementation from [33] that includes several architectural changes that enhance its performance; (c) PPO [26], a model-free policy gradient method; (d) GI-PPO [27], which performs a single RPG update epoch followed by PPO-style updates for all subsequent epochs via REINFORCE. Detailed hyper-parameters and implementation specifics for all methods are provided in Appendix C.

Metrics. We evaluate each algorithm using 12 random seeds for each task. To account for simulator stochasticity, we run each seed twice (for 24 effective runs per experiment), except in the Hopper task. Sample efficiency is evaluated via training curves in Figure 3. We report the final performance over 128 episodes using both stochastic and deterministic protocols in Table 1 and Appendix B, respectively.

5.2 Experimental Results

RPO achieves superior final performance. As summarized in Table 1, RPO consistently achieves state-of-the-art (SOTA) results across all tasks. In the challenging Hand Reorient (controlling an Allegro hand for cube rotation) and ANYmal tasks (quadruped locomotion [9]), RPO outperforms all baselines by a significant margin. Even in the Ant, Hopper, and Humanoid tasks, where baselines like SAPO and SHAC already exhibit strong performance, RPO is able to push the performance boundary further.

RPO consistently demonstrates superior sample efficiency and stability. RPO’s efficiency stems from its ability to (i) reuse samples across multiple policy updates and (ii) stabilize RPG training via the proposed clipping mechanism and KL regularization. As shown in Figure 3, these mechanisms translate to faster learning across all tasks. For instance, in Hand Reorient task, RPO learns significantly faster than all baselines.

In Hopper, RPO reaches a score of 5000 several million steps earlier than other methods. Similarly, in Ant, RPO is the fastest to reach the 8000 benchmark. In ANYmal, RPO surpasses the final performance of both SAPO and SHAC after only 4 million steps, and in Humanoid, it reaches a score of 8000 approximately 3 million steps faster than SAPO. Furthermore, RPO exhibits significantly higher sample efficiency compared to PPO across all environments.

Wall-clock Time Comparison. We investigate the computational overhead of RPO’s sample reuse mechanism in terms of wall-clock time. We compare RPO (10 million environment steps) against SHAC (40 million environment steps) on the ANYmal task. Experiments were conducted on the same machine with an NVIDIA RTX 4090 GPU, with 8 seeds evaluated sequentially. As shown in Figure 5, RPO completes training in approximately 81 minutes, whereas SHAC requires roughly 313 minutes. Notably, when training for the same duration of 10 million steps, RPO takes 80 minutes compared to 76 minutes for SHAC. This comparison reveals that sample reuse introduces only a marginal computational overhead per step. Consequently, RPO’s superior sample efficiency directly translates to wall-clock time efficiency, as SHAC fails to match RPO’s performance even with significantly longer training.

5.3 Ablation Study

In our ablation study (Figure 4), we examine the contribution of each RPO component by evaluating variants without: (i) KL regularization, (ii) gradient clipping, and (iii) sample reuse. Additionally, we analyze RPO’s hyperparameter sensitivity in Appendix I.

(i) KL regularization stabilizes policy training. KL regularization is critical for stabilizing RPO, particularly during the early training phases. As shown in Figure 4 (a), removing KL regularization significantly slows down learning; the agent reaches a score of 8000 approximately two million steps later than the full model. Further analysis of KL regularization is provided in Appendix H.

(ii) Clipping mechanism ensures numerical stability. The proposed policy gradient clipping mechanism filters out samples with large importance weight ratios. This prevents numerical instability and ensures action probabilities remain bounded. As illustrated in Figure 4 (c), removing the gradient clipping mechanism significantly degrades performance on the Hand Reorient task.

(iii) Sample reuse improves efficiency and performance. Sample efficiency degrades when limiting training to a single policy update epoch per iteration. Consequently, final performance is also compromised, as shown in Figure 4 (b), confirming the effectiveness of sample reuse.

6 Conclusion

In this work, we addressed the training instability of Reparameterization Policy Gradient by establishing a key connection between RPG and a surrogate objective. This insight provides a principled path to stable sample reuse. Based on this, we propose Reparameterization Proximal Policy Optimization, an algorithm

that stabilizes policy learning by applying a tailored gradient clipping mechanism to the surrogate objective’s policy gradient, further complemented by KL regularization. Our experiments on challenging locomotion and manipulation tasks confirm that RPO significantly outperforms prior methods in sample efficiency with strong performance. A promising direction for future work is investigating the sim-to-real transfer of RPO-trained policies.

References

- [1] Brandon Amos, Samuel Stanton, Denis Yarats, and Andrew Gordon Wilson. On the model-based stochastic value gradient for continuous reinforcement learning. In Ali Jadbabaie, John Lygeros, George J. Pappas, Pablo A. &Parrilo, Benjamin Recht, Claire J. Tomlin, and Melanie N. Zeilinger, editors, *Proceedings of the 3rd Conference on Learning for Dynamics and Control*, volume 144 of *Proceedings of Machine Learning Research*, pages 6–20. PMLR, 07 – 08 June 2021.
- [2] Feng Gao, Liangzhi Shi, Shenao Zhang, Zhaoran Wang, and Yi Wu. Adaptive-gradient policy optimization: Enhancing policy learning in non-smooth differentiable simulations. In *Forty-first International Conference on Machine Learning*, 2024.
- [3] Ignat Georgiev, Krishnan Srinivasan, Jie Xu, Eric Heiden, and Animesh Garg. Adaptive horizon actor-critic for policy learning in contact-rich differentiable simulation. In *Proceedings of the 41st International Conference on Machine Learning*, ICML’24. JMLR.org, 2024.
- [4] Geoffrey R Grimmett and David R Stirzaker. *Probability and Random Processes*. Oxford University Press, 05 2001.
- [5] Tuomas Haarnoja, Aurick Zhou, Pieter Abbeel, and Sergey Levine. Soft actor-critic: Off-policy maximum entropy deep reinforcement learning with a stochastic actor. In Jennifer Dy and Andreas Krause, editors, *Proceedings of the 35th International Conference on Machine Learning*, volume 80 of *Proceedings of Machine Learning Research*, pages 1861–1870. PMLR, 10–15 Jul 2018.
- [6] Danijar Hafner, Timothy Lillicrap, Jimmy Ba, and Mohammad Norouzi. Dream to control: Learning behaviors by latent imagination. In *International Conference on Learning Representations*, 2020.
- [7] Nicolas Heess, Gregory Wayne, David Silver, Timothy Lillicrap, Tom Erez, and Yuval Tassa. Learning continuous control policies by stochastic value gradients. In C. Cortes, N. Lawrence, D. Lee, M. Sugiyama, and R. Garnett, editors, *Advances in Neural Information Processing Systems*, volume 28. Curran Associates, Inc., 2015.
- [8] Yuanming Hu, Luke Anderson, Tzu-Mao Li, Qi Sun, Nathan Carr, Jonathan Ragan-Kelley, and Frédo Durand. DiffTaichi: Differentiable programming for physical simulation. *ICLR*, 2020.
- [9] M. Hutter, C. Gehring, A. Lauber, F. Gunther, C. D. Bellicoso, V. Tsounis, P. Fankhauser, R. Diethelm, S. Bachmann, M. Bloesch, H. Kolvenbach, M. Bjelonic, L. Isler, and K. Meyer and. Anymal - toward legged robots for harsh environments. *Advanced Robotics*, 31(17):918–931, 2017.

- [10] Sham Kakade. A natural policy gradient. In *Proceedings of the 15th International Conference on Neural Information Processing Systems: Natural and Synthetic*, NIPS'01, page 1531–1538, Cambridge, MA, USA, 2001. MIT Press.
- [11] Diederik P Kingma and Max Welling. Auto-encoding variational Bayes. In *International Conference on Learning Representations (ICLR)*, 2014.
- [12] S. Kullback and R. A. Leibler. On information and sufficiency. *The Annals of Mathematical Statistics*, 22(1):79–86, 1951.
- [13] Michel Ma, Tianwei Ni, Clement Gehring, Pierluca D'Oro, and Pierre-Luc Bacon. Do transformer world models give better policy gradients? In *Proceedings of the 41st International Conference on Machine Learning*, ICML'24. JMLR.org, 2024.
- [14] Viktor Makoviychuk, Lukasz Wawrzyniak, Yunrong Guo, Michelle Lu, Kier Storey, Miles Macklin, David Hoeller, Nikita Rudin, Arthur Allshire, Ankur Handa, and Gavriel State. Isaac gym: High performance gpu-based physics simulation for robot learning, 2021.
- [15] Luke Metz, C Daniel Freeman, Samuel S Schoenholz, and Tal Kachman. Gradients are not all you need. *arXiv preprint arXiv:2111.05803*, 2021.
- [16] Shakir Mohamed, Mihaela Rosca, Michael Figurnov, and Andriy Mnih. Monte carlo gradient estimation in machine learning. *J. Mach. Learn. Res.*, 21(1), January 2020.
- [17] Michael C. Mozer. *A focused backpropagation algorithm for temporal pattern recognition*, page 137–169. L. Erlbaum Associates Inc., USA, 1995.
- [18] Asen Nachkov, Danda Pani Paudel, Jan-Nico Zaech, Davide Scaramuzza, and Luc Van Gool. Dream to drive: Model-based vehicle control using analytic world models. *arXiv preprint arXiv:2502.10012*, 2025.
- [19] Jiahe Pan, Jiayu Xing, Rudolf Reiter, Yifan Zhai, Elie Aljalbout, and Davide Scaramuzza. Learning on the fly: Rapid policy adaptation via differentiable simulation. *IEEE Robotics and Automation Letters*, 2025.
- [20] Tao Pang, H. J. Terry Suh, Lujie Yang, and Russ Tedrake. Global planning for contact-rich manipulation via local smoothing of quasi-dynamic contact models. *IEEE Transactions on Robotics*, 39(6):4691–4711, 2023.
- [21] Paavo Parmas. Total stochastic gradient algorithms and applications in reinforcement learning. In *Proceedings of the 32nd International Conference on Neural Information Processing Systems*, NIPS'18, page 10225–10235, Red Hook, NY, USA, 2018. Curran Associates Inc.
- [22] Paavo Parmas, Carl Edward Rasmussen, Jan Peters, and Kenji Doya. PIPPS: Flexible model-based policy search robust to the curse of chaos. In Jennifer Dy and Andreas Krause, editors, *Proceedings*

- of the 35th International Conference on Machine Learning, volume 80 of *Proceedings of Machine Learning Research*, pages 4065–4074. PMLR, 10–15 Jul 2018.
- [23] Paavo Parmas, Takuma Seno, and Yuma Aoki. Model-based reinforcement learning with scalable composite policy gradient estimators. In Andreas Krause, Emma Brunskill, Kyunghyun Cho, Barbara Engelhardt, Sivan Sabato, and Jonathan Scarlett, editors, *Proceedings of the 40th International Conference on Machine Learning*, volume 202 of *Proceedings of Machine Learning Research*, pages 27346–27377. PMLR, 23–29 Jul 2023.
- [24] Danilo Jimenez Rezende, Shakir Mohamed, and Daan Wierstra. Stochastic backpropagation and approximate inference in deep generative models. In *Proceedings of The 30th International Conference on Machine Learning (ICML)*, 2014.
- [25] John Schulman, Sergey Levine, Pieter Abbeel, Michael Jordan, and Philipp Moritz. Trust region policy optimization. In Francis Bach and David Blei, editors, *Proceedings of the 32nd International Conference on Machine Learning*, volume 37 of *Proceedings of Machine Learning Research*, pages 1889–1897, Lille, France, 07–09 Jul 2015. PMLR.
- [26] John Schulman, Filip Wolski, Prafulla Dhariwal, Alec Radford, and Oleg Klimov. Proximal policy optimization algorithms. *arXiv preprint arXiv:1707.06347*, 2017.
- [27] Sanghyun Son, Laura Yu Zheng, Ryan Sullivan, Yi-Ling Qiao, and Ming Lin. Gradient informed proximal policy optimization. In *Thirty-seventh Conference on Neural Information Processing Systems*, 2023.
- [28] Yunlong Song, Sang bae Kim, and Davide Scaramuzza. Learning quadruped locomotion using differentiable simulation. In *8th Annual Conference on Robot Learning*, 2024.
- [29] Hyung Ju Suh, Max Simchowitz, Kaiqing Zhang, and Russ Tedrake. Do differentiable simulators give better policy gradients? In Kamalika Chaudhuri, Stefanie Jegelka, Le Song, Csaba Szepesvari, Gang Niu, and Sivan Sabato, editors, *Proceedings of the 39th International Conference on Machine Learning*, volume 162 of *Proceedings of Machine Learning Research*, pages 20668–20696. PMLR, 17–23 Jul 2022.
- [30] Richard S. Sutton and Andrew G. Barto. *Reinforcement Learning: An Introduction*. A Bradford Book, Cambridge, MA, USA, 2018.
- [31] Richard S Sutton, David McAllester, Satinder Singh, and Yishay Mansour. Policy gradient methods for reinforcement learning with function approximation. In S. Solla, T. Leen, and K. Müller, editors, *Advances in Neural Information Processing Systems*, volume 12. MIT Press, 1999.
- [32] Ronald J Williams. Simple statistical gradient-following algorithms for connectionist reinforcement learning. *Machine learning*, 8:229–256, 1992.
- [33] Eliot Xing, Vernon Luk, and Jean Oh. Stabilizing reinforcement learning in differentiable multiphysics simulation. In *The Thirteenth International Conference on Learning Representations*, 2025.

- [34] Jie Xu, Viktor Makoviychuk, Yashraj Narang, Fabio Ramos, Wojciech Matusik, Animesh Garg, and Miles Macklin. Accelerated policy learning with parallel differentiable simulation. In *International Conference on Learning Representations*, 2021.
- [35] Haoxiang You, Yilang Liu, and Ian Abraham. Accelerating visual-policy learning through parallel differentiable simulation. In *The Thirty-ninth Annual Conference on Neural Information Processing Systems*, 2025.
- [36] Shenao Zhang, Wanxin Jin, and Zhaoran Wang. Adaptive barrier smoothing for first-order policy gradient with contact dynamics. In *Proceedings of the 40th International Conference on Machine Learning, ICML'23*. JMLR.org, 2023.
- [37] Shenao Zhang, Boyi Liu, Zhaoran Wang, and Tuo Zhao. Model-based reparameterization policy gradient methods: Theory and practical algorithms. In A. Oh, T. Naumann, A. Globerson, K. Saenko, M. Hardt, and S. Levine, editors, *Advances in Neural Information Processing Systems*, volume 36, pages 68391–68419. Curran Associates, Inc., 2023.
- [38] Xiaoyuan Zhang, Xinyan Cai, Bo Liu, Weidong Huang, Song-Chun Zhu, Siyuan Qi, and Yaodong Yang. Differentiable information enhanced model-based reinforcement learning. *Proceedings of the AAAI Conference on Artificial Intelligence*, 39(21):22605–22613, Apr. 2025.
- [39] Yuang Zhang, Yu Hu, Yunlong Song, Danping Zou, and Weiyao Lin. Back to newton’s laws: Learning vision-based agile flight via differentiable physics. *arXiv preprint arXiv:2407.10648*, 2024.
- [40] Yaofeng Desmond Zhong, Jiequn Han, Biswadip Dey, and Georgia Olympia Brikis. Improving gradient computation for differentiable physics simulation with contacts. In Nikolai Matni, Manfred Morari, and George J. Pappas, editors, *Proceedings of The 5th Annual Learning for Dynamics and Control Conference*, volume 211 of *Proceedings of Machine Learning Research*, pages 128–141. PMLR, 15–16 Jun 2023.

A Environment and Task details

In this section, we discuss the details of the environments and tasks used in this work. The four locomotion tasks (i.e., Anymal, Hopper, Ant, and Humanoid) are from the DFlex simulator [34, 3]. Specifically, we use the versions from AHAC’s official implementation (<https://github.com/imgeorgiev/DiffRL>). All locomotion tasks aim to learn a policy that maximizes the agent’s forward velocity. The Hand Reorient task is from the official implementation of Rewarped (<https://github.com/rewarped/rewarped>), version 1.3.0.

A.1 Ant

Ant ($S \in \mathbb{R}^{37}$, $A \in \mathbb{R}^8$) is a four-legged robot. The reward function is defined as [3]:

$$v_x + R_{height} + 0.1R_{angle} + R_{heading} - 0.01\|a\|^2,$$

where v_x is the forward velocity, and the other components are: R_{height} , which encourages the robot to stand up; R_{angle} , which rewards an upward-pointing normal vector; $R_{heading}$, which promotes forward movement; and a penalty on the action norm, $-0.01\|a\|^2$, to encourage energy-efficient policies.

A.2 Anymal

Anymal ($S \in \mathbb{R}^{49}$, $A \in \mathbb{R}^{12}$) is a real quadrupedal robot [9]. The reward function is defined as [3]:

$$v_x + R_{height} + 0.1R_{angle} + R_{heading} - 0.01\|a\|^2.$$

A.3 Hopper

Hopper ($S \in \mathbb{R}^{11}$, $A \in \mathbb{R}^3$) is a three-jointed planar robot. The reward function is defined as [3]:

$$v_x + R_{height} + R_{angle} - 0.1\|a\|^2.$$

A.4 Humanoid

Humanoid ($S \in \mathbb{R}^{76}$, $A \in \mathbb{R}^{21}$) is a high-dimensional bipedal robot. The reward function is defined as [3]:

$$v_x + R_{height} + 0.1R_{angle} + R_{heading} - 0.02\|a\|^2.$$

A.5 Hand Reorient

This task involves an Allegro Hand ($S \in \mathbb{R}^{72}$, $A \in \mathbb{R}^{16}$) learning to reorient a cube to a target pose. This task was adapted for Rewarped [33] from Isaac Gym [14]. The detailed reward function can be found in the original Isaac Gym paper [14].

Table 2: Common hyperparameters for all algorithms.

	<i>shared</i>	PPO	SHAC	SAPO	RPO	GI-PPO
Horizon H	32					
Epochs for critics L		5	16	16	16	16
Epochs for actors M		5	1	1	5	6
Discount γ	0.99					
TD/GAE λ	0.95					
Actor MLP	(400, 200, 100)	shared actor-critic MLP				
Critic MLP	(400, 200, 100)	shared actor-critic MLP				
Actor η		$5e-4$	$2e-3$	$2e-3$	$5e-4$	$5e-4$
Critic η	$5e-4$					
Entropy η	-			$5e-3$		
η schedule	-	KL(0.008)	linear	linear	exponential	N.A.
Optim type	AdamW					
Optim (β_1, β_2)	(0.7, 0.95)	(0.9, 0.999)				
Grad clip	0.5					1.0
Norm type	LayerNorm					
Activation type	SiLU					
Num critics C	-		2	2	2	2
Target entropy $\bar{\mathcal{H}}$	-			$-\dim(\mathcal{A})/2$	$-\dim(\mathcal{A})/2$	
Init temperature	-			1.0 (0.005 for Hand Reorient)		

Table 3: The number of parallel environments used for each environment. These values are kept the same as in the official implementations: we follow the AHAC repository (<https://github.com/imgeorgiev/DiffRL>) for the DFlex tasks and the Rewarped repository (<https://github.com/rewarped/rewarped>) for the Hand Reorient task.

	Hopper	Ant	Humanoid	Anymal	Hand Reorient
Num Envs	1024	128	64	128	64

Table 4: RPO’s unique hyperparameters.

	Hopper	Ant	Humanoid	Anymal	Hand Reorient
Entropy coefficient	0.25	0.2	0.5	0.25	0.001
KL coefficient	0.2	0.25	0.5	0.2	0.003
c_{low}	0.8	0.8	0.8	0.8	0.8
c_{high}	1.0	1.0	1.0	1.0	1.0

Table 5: GI-PPO’s unique hyperparameters.

	Hopper	Ant	Humanoid	Anymal	Hand Reorient
alpha	$5e-1$	$5e-1$	$5e-3$	$1e-3$	$5e-4$
max oorr	0.7	0.8	0.1	0.5	0.1
e clip	0.2	0.2	0.2	0.2	0.05
alpha interval	0.4	0.4	0.4	0.4	0.4
alpha update factor	1.02	1.02	1.02	1.02	1.02

Table 6: Deterministic Evaluation for the final performance after training. Each evaluation consists of 128 episodes. Mean and standard deviation.

	Hand Reorient	Hopper	Ant	Humanoid	Anymal
PPO	37.18 \pm 12.76	3977.85 \pm 159.95	4339.51 \pm 745.48	2140.61 \pm 529.07	10257.12 \pm 2247.05
GI-PPO	36.78 \pm 20.90	5514.00 \pm 285.64	7812.05 \pm 1165.10	7576.97 \pm 621.58	12247.36 \pm 3552.17
SHAC	175.13 \pm 55.10	5068.42 \pm 299.73	8205.95 \pm 940.18	7722.20 \pm 742.96	14560.59 \pm 655.30
SAPO	225.17 \pm 27.66	5478.12 \pm 4.45	9101.36 \pm 996.14	8676.25 \pm 420.62	14783.27 \pm 53.01
RPO (ours)	239.70 \pm 19.77	5584.86 \pm 6.41	9072.29 \pm 448.57	8805.61 \pm 361.59	15872.61 \pm 461.15

B Deterministic Evaluation results

In this section, we provide the deterministic evaluation results for the five tasks used in the paper. For stochastic evaluations, we sample actions from the policy distribution. Results are shown in Table 6. As shown in Table 6, RPO achieves best results across tasks.

C Hyperparameters and Implementation Details

C.1 Hyperparameters and Architectures

We detail the hyperparameters and architectures used for all algorithms in Table 2. For our GI-PPO baseline, we followed the official implementation (<https://github.com/SonSang/gippo>) but made several improvements. These changes include using a double critic architecture, switching from the Adam to the AdamW optimizer, aligning the network size with our method, and changing the activation function from ELU to SiLU. Since GI-PPO is sensitive to its hyperparameters, we performed an extensive search within our computational budget. The resulting hyperparameters used are listed in Table 5. Our implementations of SAPO, PPO, and SHAC are based on the official SAPO repository (<https://github.com/etaoxing/mineral>). Most hyperparameters are kept consistent with that repository, with a few key exceptions for fair comparison: the number of parallel environments and the MLP size are aligned with the official AHAC repository [3]. To ensure a fair comparison, most hyperparameters and the core architecture are shared across all tested algorithms. We tuned the initial temperature for SAPO in the Hand Reorient task, as the default setting (i.e, in SAPO’s paper for this task) of 1.0 from the SAPO paper was found to be too high. Specifically for SHAC, we use the improved version from the SAPO repository, which aligns its architecture with that of RPO and SAPO. Our RPO implementation is also built upon the SAPO repository.

C.2 Implementation Details for RPO

For the critic, we use double critic and mean average as target for TD training, following [33]. For the entropy regularization, we follow SAPO to add an entropy bonus to the reward, which is scaled by a target entropy [33].

D Details and proofs for Connecting RPG and Surrogate Objective

In this section, we give details to explain the connection between RPG and surrogate objective. First, we rewrite equation 8 by expanding $d^{\pi_{\theta_{\text{old}}}}(s)$ and interchanging the order of integration and summation:

$$\begin{aligned}
 \nabla_{\theta} L_{\pi_{\theta_{\text{old}}}}(\theta) &= \int_s d^{\pi_{\theta_{\text{old}}}}(s) \int_{\epsilon} [\nabla_{\theta} a \nabla_a Q^{\pi_{\theta_{\text{old}}}}(s, a)|_{a=f_{\theta}(\epsilon; s)} p_{\text{std}}(\epsilon)] d\epsilon \, ds, \\
 &= \int_s \sum_{t=0}^{\infty} \gamma^t p(s_t = s | \pi_{\theta_{\text{old}}}) \int_{\epsilon} [\nabla_{\theta} a \nabla_a Q^{\pi_{\theta_{\text{old}}}}(s, a)|_{a=f_{\theta}(\epsilon; s)} p_{\text{std}}(\epsilon)] d\epsilon \, ds, \\
 &= \sum_{t=0}^{\infty} \int_s \gamma^t p(s_t = s | \pi_{\theta_{\text{old}}}) \int_{\epsilon} [\nabla_{\theta} a \nabla_a Q^{\pi_{\theta_{\text{old}}}}(s, a)|_{a=f_{\theta}(\epsilon; s)} p_{\text{std}}(\epsilon)] d\epsilon \, ds,
 \end{aligned} \tag{16}$$

which is the policy gradient to be estimated and $p_{\text{std}}(\epsilon)$ is the probability density function for standard Gaussian distribution.

D.1 Collect rollouts and compute action-gradients

First, as shown in Section 4.1.1, we collect a batch of rollouts and compute the gradients of discounted cumulative return with respect to the action at each time step with BPTT. From here, we clearly see that the action-gradient for time step k , $\gamma^k \nabla_{a_k} \sum_{t=k}^{\infty} \gamma^{(t-k)} r(s_t, a_t)$, is exactly an unbiased Monte Carlo estimate of $\gamma^k \nabla_a Q^{\pi_{\theta_{\text{old}}}}(s_k, a_k)$, where s_k and a_k are sampled according to $p(s_k = s | \pi_{\theta_{\text{old}}})$ and $\pi_{\theta_{\text{old}}}(a|s)$. We cache these action-gradients for further calculations.

D.2 On-Policy Gradient

Now, we are ready to compute the reparameterization gradients. For the first policy update (on-policy update), the behavior policy $\pi_{\theta_{\text{old}}}$ is the same as the policy π_{θ} being updated. We can backpropagate the gradients from the action to the policy network parameters θ . Then, we get an unbiased Monte Carlo estimate of $\int_s \gamma^k p(s_k = s | \pi_{\theta_{\text{old}}}) \int_{\epsilon} [\nabla_{\theta} a \nabla_a Q^{\pi_{\theta_{\text{old}}}}(s, a)|_{a=f_{\theta}(\epsilon; s)} p_{\text{std}}(\epsilon)] d\epsilon ds$. This holds true, as s_k is sampled according to $p(s_k = s | \pi_{\theta_{\text{old}}})$, a_k is generated by sampling $\epsilon \sim p_{\text{std}}(\epsilon)$ and then applying the transformation $a_k = f_{\theta_{\text{old}}}(\epsilon; s_k)$, and $\pi_{\theta_{\text{old}}}$ coincides with π_{θ} for this policy update epoch.

By summing the gradients over different time steps and averaging across different trajectories, we obtain an unbiased on-policy reparameterization gradient estimation for equation 16.

D.3 Off-policy Gradient

After the first policy update, π_{θ} is updated to $\pi_{\theta'}$, and we need to compute off-policy gradients. To do so, we need to account for the fact that to regenerate the same action collected in the rollout, a different sampled noise ϵ_{reg} is required for θ' .

To generate the sampled action a_k , ϵ_{reg} and ϵ are linked by the following relation:

$$a_k = f_{\theta_{\text{old}}}(\epsilon; s_k) = f_{\theta'}(\epsilon_{\text{reg}}; s_k). \quad (17)$$

Since we consider reparameterization Gaussian transformations in this work, $f_{\theta_{\text{old}}}$ and $f_{\theta'}$ are invertible. We can therefore compute $\epsilon_{\text{reg}} = f_{\theta'}^{-1}(a_k; s_k)$ and then regenerate a_k with the updated policy $\pi_{\theta'}$. Now, we backpropagate cached action-gradients to policy network parameters θ' and obtain an unbiased estimation of $\gamma^k \nabla_{\theta'} a_k \nabla_{a_k} Q^{\pi_{\theta_{\text{old}}}}(s_k, a_k)|_{a_k=f_{\theta'}(\epsilon_{\text{reg}}; s_k)}$.

However, instead of sampling ϵ_{reg} directly from $\mathcal{N}(0, \mathcal{I})$, we sample it as $\epsilon_{\text{reg}} = f_{\theta'}^{-1}(f_{\theta_{\text{old}}}(\epsilon; s_k); s_k)$, where ϵ is sampled from $\mathcal{N}(0, \mathcal{I})$. Hence, the probability density $p_{\text{reg}}(\epsilon_{\text{reg}})$ is different from standard Gaussian. We therefore multiply the computed gradient term $\gamma^k \nabla_{\theta'} a_k \nabla_{a_k} Q^{\pi_{\theta_{\text{old}}}}(s_k, a_k)|_{a_k=f_{\theta'}(\epsilon_{\text{reg}}; s_k)}$ by the importance ratio $\rho(\theta') = \frac{\pi_{\theta'}(a_k|s_k)}{\pi_{\theta_{\text{old}}}(a_k|s_k)}$ to obtain an unbiased off-policy gradient estimate. We now show that weighting by this importance weight ratio, we indeed obtain an unbiased estimate of the target gradient: $\int_s \gamma^k p(s_k = s | \pi_{\theta_{\text{old}}}) \int_{\epsilon} [\nabla_{\theta'} a \nabla_a Q^{\pi_{\theta_{\text{old}}}}(s, a)|_{a=f_{\theta'}(\epsilon; s)} p_{\text{std}}(\epsilon)] d\epsilon ds$.

Proposition 1. *Let the state s_k be sampled from the state distribution of the behavior policy, $s_k \sim p(s_k = s | \pi_{\theta_{\text{old}}})$. Let the reparameterization noise ϵ be sampled from the standard Normal distribution, $\epsilon \sim p_{\text{std}}(\epsilon)$, and define the regenerated noise as $\epsilon_{\text{reg}} = f_{\theta'}^{-1}(f_{\theta_{\text{old}}}(\epsilon; s_k); s_k)$, where $f_{\theta'}$ and $f_{\theta_{\text{old}}}$ are reparameterization Gaussian transformations.*

Define the off-policy gradient estimator $G(\theta')$ as the random variable:

$$G(\theta') = \gamma^k \frac{\pi_{\theta'}(a_k|s_k)}{\pi_{\theta_{\text{old}}}(a_k|s_k)} \nabla_{\theta'} a_k \nabla_{a_k} Q^{\pi_{\theta_{\text{old}}}}(s_k, a_k)|_{a_k=f_{\theta'}(\epsilon_{\text{reg}}; s_k)}$$

where the action $a_k = f_{\theta_{\text{old}}}(\epsilon; s_k) = f_{\theta'}(\epsilon_{\text{reg}}; s_k)$.

Then, $G(\theta')$ is an unbiased estimate of the true policy gradient. That is, its expectation over the distributions of s_k and ϵ is given by:

$$\mathbb{E}_{s_k, \epsilon} [G(\theta')] = \int_s \gamma^k p(s_k = s | \pi_{\theta_{\text{old}}}) \int_{\epsilon} [\nabla_{\theta'} a \nabla_a Q^{\pi_{\theta_{\text{old}}}}(s_k, a)|_{a=f_{\theta'}(\epsilon; s_k)} p_{\text{std}}(\epsilon)] d\epsilon ds$$

Proof. We first consider the case where the action $a \in \mathbb{R}$ is a scalar, and then generalize the result to the multi-dimensional case.

Since ϵ_{reg} is sampled as $\epsilon_{\text{reg}} = f_{\theta'}^{-1}(f_{\theta_{\text{old}}}(\epsilon; s_k); s_k)$, $f_{\theta'}$ and $f_{\theta_{\text{old}}}$ are differentiable and monotonically increasing with respect to ϵ_{reg} and ϵ , we can calculate the probability density function $p_{\text{reg}}(\epsilon_{\text{reg}})$ by the change of variable formula [4]:

$$p_{\text{reg}}(\epsilon_{\text{reg}}) = p_{\text{std}}(\epsilon) \frac{df_{\theta_{\text{old}}}^{-1}(a_k; s_k)}{da_k} \frac{df_{\theta'}(\epsilon_{\text{reg}}; s_k)}{d\epsilon_{\text{reg}}}.$$

We also know that the importance weight ratio has the following specific form:

$$\frac{\pi_{\theta'}(a_k|s_k)}{\pi_{\theta_{\text{old}}}(a_k|s_k)} = \frac{p_{\text{std}}(\epsilon_{\text{reg}})}{p_{\text{std}}(\epsilon)} \frac{\frac{df_{\theta'}^{-1}(a_k;s_k)}{da_k}}{\frac{df_{\theta_{\text{old}}}^{-1}(a_k;s_k)}{da_k}},$$

since $a_k = f_{\theta_{\text{old}}}(\epsilon; s_k) = f_{\theta'}(\epsilon_{\text{reg}}; s_k)$, where ϵ and ϵ_{reg} are both sampled from standard Gaussian distributions, and applying the change of variable formula.

Now, we take the expectation of $G(\theta')$ with respect to ϵ_{reg} with probability density function p_{reg} :

$$\begin{aligned} & \gamma^k \int_{\epsilon_{\text{reg}}} \left[\frac{\pi_{\theta'}(a_k|s_k)}{\pi_{\theta_{\text{old}}}(a_k|s_k)} \nabla_{\theta'} a \nabla_a Q^{\pi_{\theta_{\text{old}}}}(s, a) \Big|_{a=f_{\theta'}(\epsilon_{\text{reg}}; s)} p_{\text{reg}}(\epsilon_{\text{reg}}) d\epsilon_{\text{reg}} \right] \\ &= \gamma^k \int_{\epsilon_{\text{reg}}} \left[\frac{p_{\text{std}}(\epsilon_{\text{reg}})}{p_{\text{std}}(\epsilon)} \frac{\frac{df_{\theta'}^{-1}(a_k;s_k)}{da_k}}{\frac{df_{\theta_{\text{old}}}^{-1}(a_k;s_k)}{da_k}} \nabla_{\theta'} a \nabla_a Q^{\pi_{\theta_{\text{old}}}}(s, a) \Big|_{a=f_{\theta'}(\epsilon_{\text{reg}}; s)} \right. \\ & \quad \left. \cdot p_{\text{std}}(\epsilon) \frac{df_{\theta_{\text{old}}}^{-1}(a_k; s_k)}{da_k} \frac{df_{\theta'}(\epsilon_{\text{reg}}; s_k)}{d\epsilon_{\text{reg}}} d\epsilon_{\text{reg}} \right] \\ &= \gamma^k \int_{\epsilon_{\text{reg}}} \left[\nabla_{\theta'} a \nabla_a Q^{\pi_{\theta_{\text{old}}}}(s, a) \Big|_{a=f_{\theta'}(\epsilon_{\text{reg}}; s)} p_{\text{std}}(\epsilon_{\text{reg}}) d\epsilon_{\text{reg}} \right], \end{aligned}$$

where the product of the derivatives $\frac{df_{\theta'}^{-1}(a_k;s_k)}{da_k}$ and $\frac{df_{\theta'}(\epsilon_{\text{reg}};s_k)}{d\epsilon_{\text{reg}}}$ is 1, as the functions are inverses. We can clearly see that this expectation matches our target, providing an unbiased estimate.

The extension of this result to the multi-dimensional case is straightforward. Since the source of randomness is a standard Gaussian distribution, each dimension is sampled independently. Consequently, both the overall importance ratio and $p_{\text{reg}}(\epsilon_{\text{reg}})$ factorize into a product of their respective one-dimensional components. Recalling that states are sampled according to $p(s_k = s | \pi_{\theta_{\text{old}}})$, and by moving γ^k to the outer integral, we can conclude that this method provides an unbiased estimate of

$$\int_s \gamma^k p(s_k = s | \pi_{\theta_{\text{old}}}) \int_{\epsilon} \left[\nabla_{\theta'} a \nabla_a Q^{\pi_{\theta_{\text{old}}}}(s_k, a) \Big|_{a=f_{\theta'}(\epsilon; s_k)} p_{\text{std}}(\epsilon) d\epsilon \right] ds.$$

□

Thanks to proposition 1, by summing over different time step and averaging across different trajectories, we obtain an unbiased off-policy reparameterization gradient estimation.

E Ablation Experiments on Learning Rate

RPO utilizes an exponential learning rate decay schedule. This strategy leverages RPO's high sample efficiency for rapid initial learning, while the decaying rate accelerates final convergence. We investigate the effect of applying this exact same exponential schedule to SAPO. We evaluate two variants of SAPO with

initial actor learning rates of 5×10^{-4} and 2×10^{-3} (SAPO's default). As shown in Figure 6, RPO consistently outperforms SAPO under both settings.

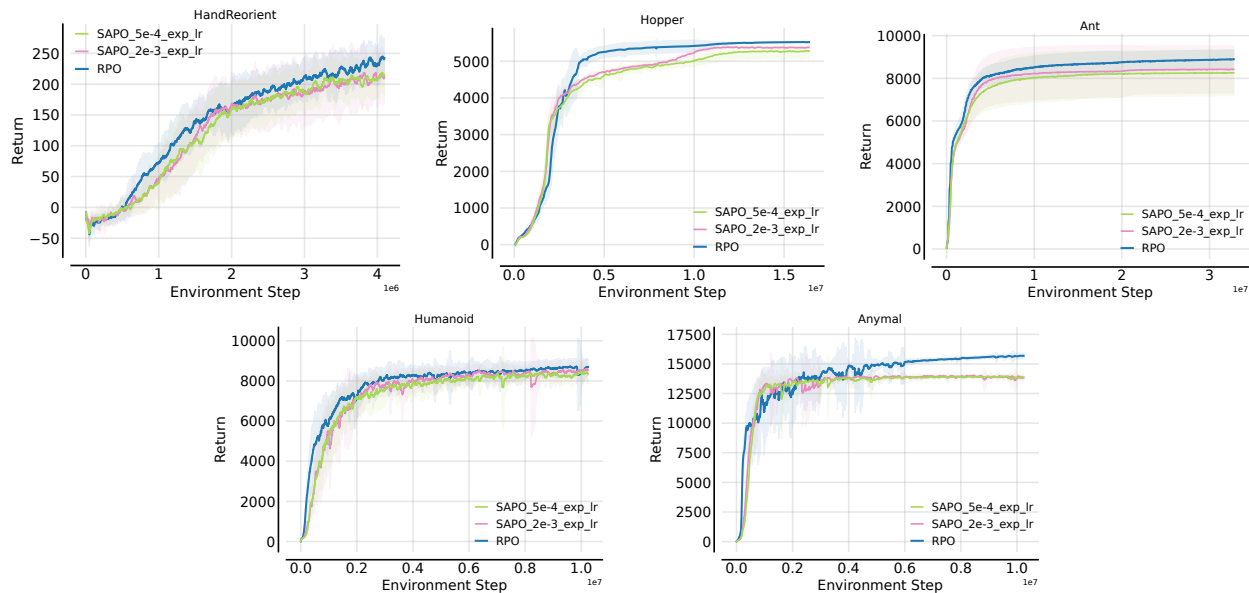


Figure 6: Ablation study comparing RPO and SAPO with an exponential learning rate schedule. We evaluate SAPO with initial actor learning rates of 5×10^{-4} and 2×10^{-3} (default setting).

F RPO’s Effective Sample Ratio

In this section, we analyze the sample utilization efficiency of RPO by measuring the proportion of samples that are not filtered out by the gradient clipping mechanism. We define the *effective sample ratio* as the percentage of samples whose gradients are not zeroed out during the off-policy update epochs (specifically, epochs 2 to 5). Note that in the first epoch, all samples are effective by definition. The results are presented in Figure 7. As shown in the figure, RPO maintains a high effective sample ratio; the lowest observed ratio is approximately 70%, which gradually approaches 100% towards the end of training.

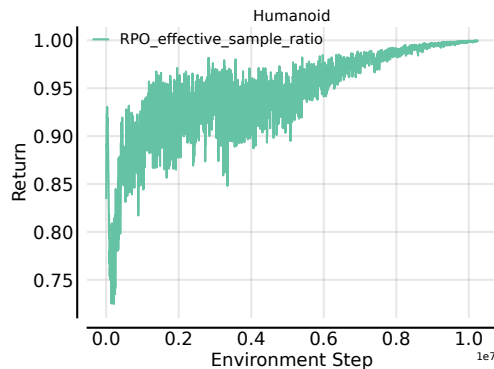


Figure 7: RPO’s effective sample ratio on Humanoid Task.

G More Comparisons with Baselines

G.1 Comparison with Soft Actor-Critic

We compare RPO with Soft Actor-Critic (SAC) [5], incorporating the n-step return mechanism for critic training, on two tasks: Anymal and Humanoid. We utilize the implementation from the Mineral repository (<https://github.com/etaoxing/mineral>) and align the actor and critic MLP hidden layers to [400, 200, 100]. We tuned SAC’s hyperparameters, including the n-step horizon, target critic smoothing coefficient, and actor learning rate, as detailed in Table 7. The training curves are presented in Figure 8. The results demonstrate that RPO consistently outperforms SAC.

Table 7: Hyperparameters for SAC.

	Humanoid	Anymal
n-step	3	10
actor learning rate	$5e - 4$	$2e - 3$
target critic smoothing coefficient	0.2	0.6

G.2 Comparison with PPO Trained on More Samples

It is well known that PPO, due to its reliance on REINFORCE-type policy gradients, is much less sample-efficient than RPG-based approaches [16, 34]. We trained PPO on the Hopper task with 200 million envi-

ronment steps and on the Anymal task with 100 million environment steps. The results show that even with 10 times more interactions with the environment, RPO still achieves a higher reward than PPO. The training curves are shown in Figure 9.

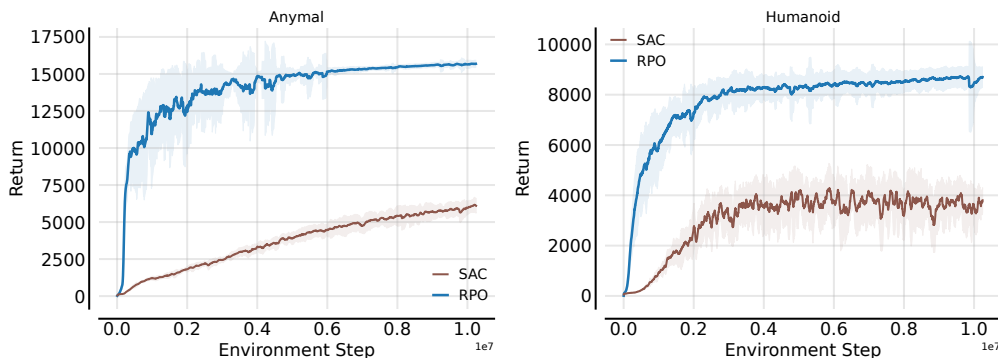


Figure 8: Ablation study for comparison of RPO and SAC.

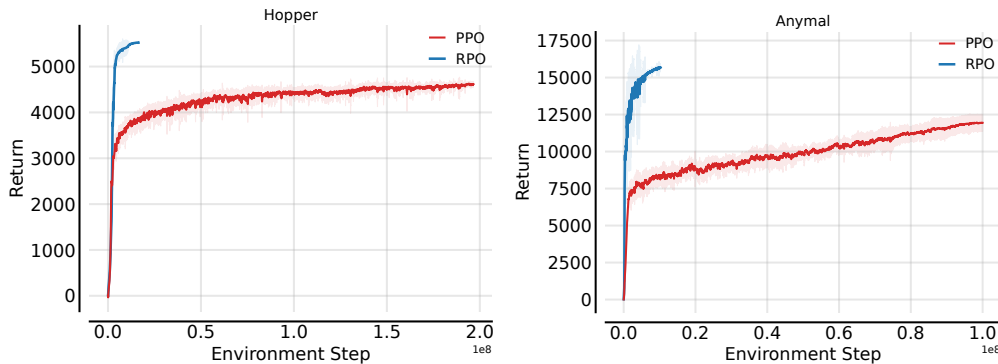


Figure 9: Comparison between RPO and PPO trained on significantly more samples.

H More Ablation on KL Divergence Regularization

We conducted further ablation studies on RPO without KL divergence regularization on the Hopper task to isolate its impact. The training curves are presented in Figure 10. As discussed in the main text, RPO without KL regularization learns noticeably more slowly than standard RPO. This retardation is primarily due to unstable policy updates.

I Hyperparameter Sensitivity Analysis

We conducted extensive experiments on the Anymal task to rigorously test RPO’s sensitivity to key hyperparameters. Specifically, we evaluated the impact of variations in: (i) the policy gradient clipping bounds (c_{low} and c_{high}); and (ii) different combinations of KL regularization (λ_{KL}) and entropy (λ_{ent}) coefficients. The corresponding training curves are visualized in Figure 11.

The results demonstrate that RPO exhibits strong robustness across a wide range of hyperparameter settings. Regarding clipping values, both stricter and looser bounds yield performance comparable to the default

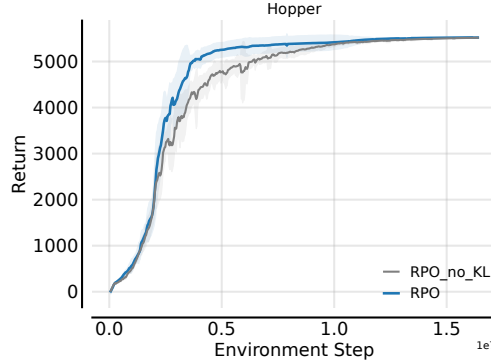


Figure 10: Ablation study for RPO without KL regularization on the Hopper task.

setting, indicating that the algorithm is not brittle to precise clipping thresholds. Also, RPO can achieve good performance with a range of KL and entropy coefficients.

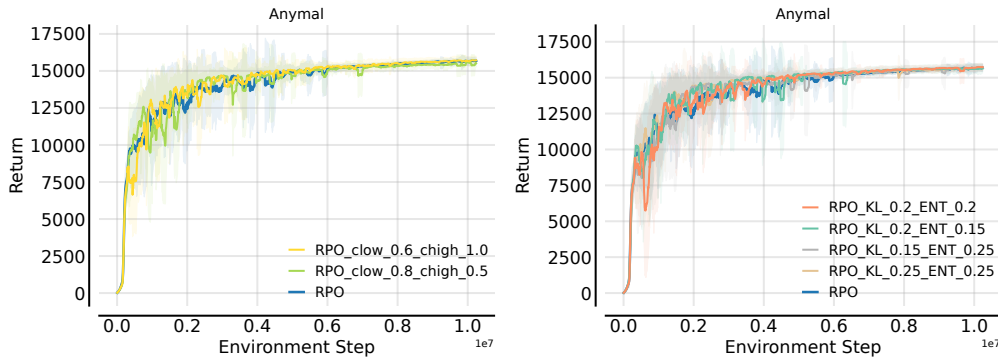


Figure 11: Ablation study on clipping values and KL/entropy coefficients.

J Discussion on the Design Choices of KL Regularization and Policy Gradient Clipping

In this section, we discuss the rationale behind using both KL regularization and the policy gradient clipping mechanism to stabilize policy training.

The clipping mechanism alone is insufficient to stabilize training and reduces the effective sample reuse ratio, whereas KL regularization stabilizes training without sacrificing sample reuse. To demonstrate this, we conducted experiments on the Humanoid task for RPO without the KL loss, using stricter clipping settings of $c_{low} = 0.1, c_{high} = 0.1$ and $c_{low} = 0.2, c_{high} = 0.2$, respectively. As shown in Figure 12, even with small clipping ranges, policy updates remain unstable. Furthermore, strict clipping limits the degree of sample reuse. We define the *effective sample ratio* as the percentage of samples whose gradients are not zeroed out during the off-policy update epochs (specifically, epochs 2 to 5). Both small clipping settings result in a very low effective sample ratio during the early phase of training. These limitations translate to a degradation in learning speed, which hurts sample efficiency. On the other hand, KL regularization allows us to explicitly regularize policy updates, leading to stable updates while enabling maximal and stable

sample reuse.

The clipping mechanism is still necessary alongside KL regularization to filter out large importance weight ratios. As shown in Figure 12, importance weight ratios can be large. Hence, it is natural to incorporate a gradient clipping mechanism to prevent policy updates driven by extreme importance weight ratios and to prevent the probability ratio of certain actions from becoming too low. Additionally, since we must calculate the importance weight ratio for unbiased policy gradient estimation regardless, there is minimal computational overhead in incorporating the policy gradient clipping mechanism.

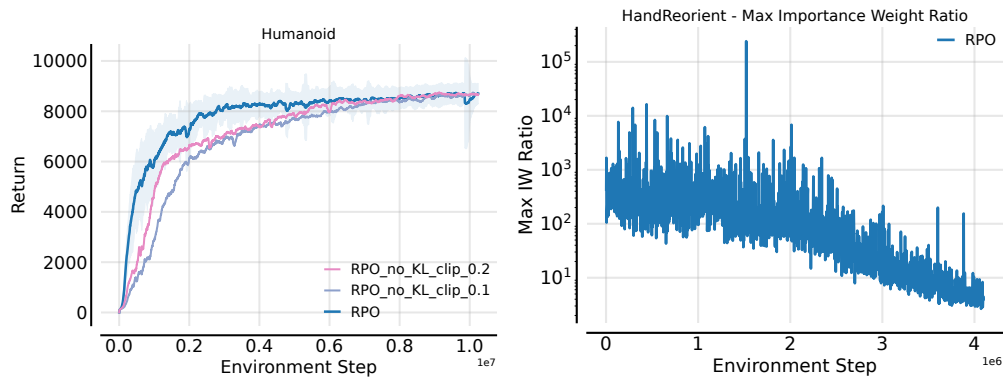


Figure 12: (a) Comparison of return, between RPO and RPO without KL regularization (using stricter clipping values). (b) We measure the average max importance weight ratios for policy update epochs 2 to 4.

K More examples for instability of RPG-based Methods

In this section, we show examples of unstable seeds for SAPO and SHAC, which are summarized in Figure 13 and Figure 14.

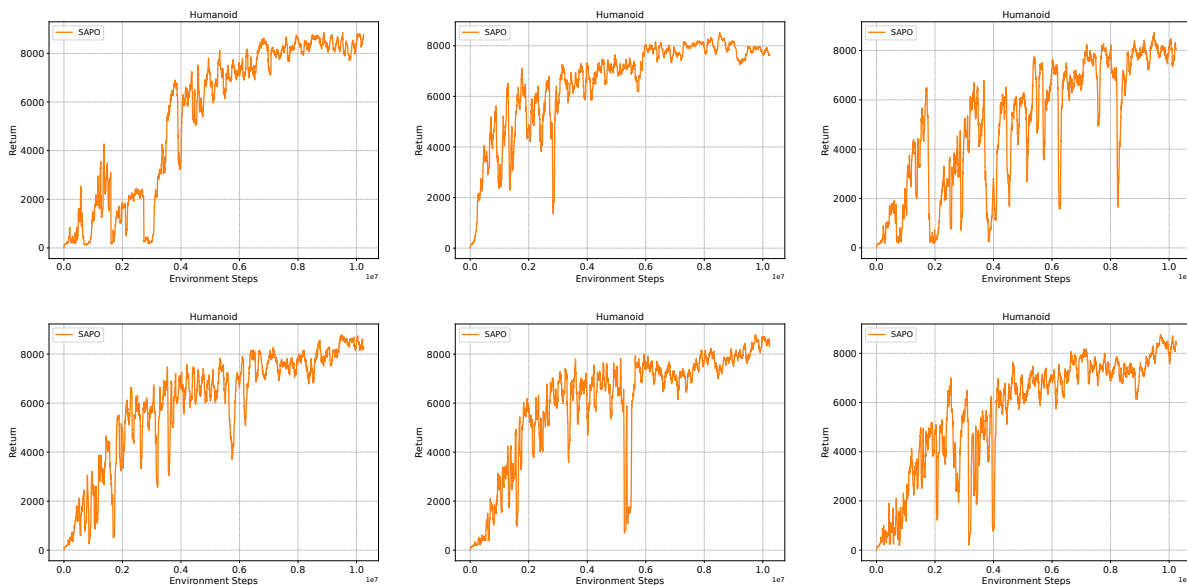


Figure 13: Unstable Seeds for SAPO on the Humanoid tasks.

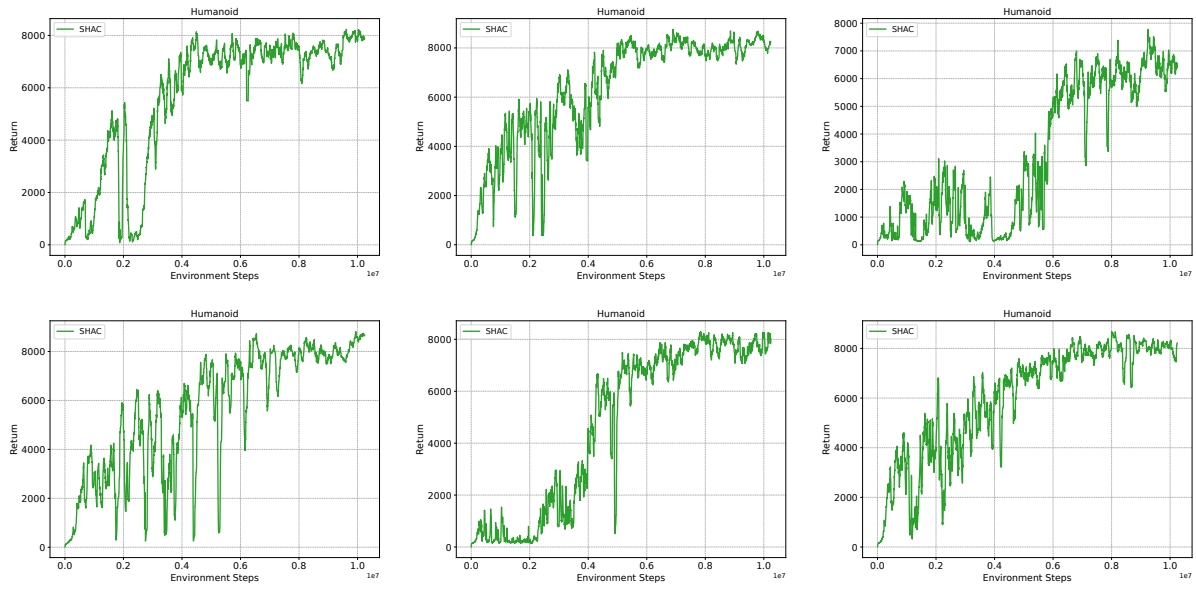


Figure 14: Unstable Seeds for SHAC on the Humanoid tasks.